The Effect of Proton Irradiation on the Corrosion Behaviors of Ferritic/Martensitic Steel in Liquid Metal Environment

Jeonghyeon Lee[1], Taeyong Kim[1], Sang Hun Shin[2] and Ji Hyun Kim[1]*

[1]Ulsan National Institute Science and Technology (UNIST), Ulsan, Republic of Korea

[2]Korea Atomic Energy Research Institute (KAERI), Daejeon, Republic of Korea

E-mail contact of main author: kimjh@unist.ac.kr

Abstract. Ferritic-martensitic steel (FMS), which contains 9-12 wt.% of chromium, is being considered as an attractive candidate material for a fuel cladding of a sodium-cooled fast reactor (SFR) due to their high thermal conductivity, low thermal expansion coefficient, and excellent irradiation resistances to void swelling compared to austenitic stainless steels. Gr. 92 steel (9Cr-0.5Mo-1.8W-VNb) is the one of advanced versions of high chromium steels that was developed in the early 1990s. It has a higher creep-rupture strength than predecessors, 9Cr-1Mo steel and Gr. 91 steel (9Cr-1Mo-VNb). Thus, it is suitable for high temperature applications in advanced reactors since it can be used even above 650°C. While nuclear reactor is under operation, structural materials of cladding have been irradiated by neutron as well as various types of ion beams which can induce some damage on the material. Proton irradiation has been used for the past few decades to simulate neutron damages, because protons have a higher scattering cross-section than fast neutrons and it can form displacements This study is aimed at investigating the irradiation effects on corrosion behavior of FMS using accelerated technique, the proton irradiation, to understand irradiation situation of cladding materials during its life time inside of the core. The non-irradiated and irradiated FMS materials were used for corrosion and dissolution experiments. Through the experiments, it was observed that the irradiated materials exhibit worse corrosion and dissolution compared to the non-irradiated one.

Key Words: Sodium, Ferritic/Martensitic steel, corrosion, irradiation

1. Introduction

Liquid metal fast breeder reactors (LMFBRs) such as the sodium-cooled fast reactor (SFR) and the lead-cooled fast reactor (LFR) are candidates among GEN-IV nuclear energy systems. Among the various liquid metals that can be used to a primary coolant materials, and sodium is a world widrly used coolant in the design of Gen-IV reactors [1]. As a coolant for fast reactor systems, liquid sodium provide some advantages over liquid lead or lead-bismuth eutectic (LBE). First, LBE makes the materials corrosion that the solubility of steel materials is larger into LBE. Second, LBE has the radiological hazards associated with coolant activation. Polonium 210 is produced from the Bi by neutron reaction. As a result polonium is retained in the lead-bismuth eutectic during normal operating conditions and can cause problems only if coolant leakage through the steam generator or the vessel occurs [2].

However, the sodium has 100 times more effective heat transfer medium compared to water and wide temperature margin about 400 °C to boiling. Sodium features a reasonably low melting temperature, but also a low boiling point (883 °C), which raises safety concerns regarding unprotected transients leading to a coolant heatup. And, LBE or lead coolant velocity is limited by erosion concerns of protective oxide layers to about 2.5–3.0 m/s. Typical sodium velocities are up to 8–10 m/s, hence lead has, in practice, a lower heat removal capacity. And, These features together with the higher flow velocity of sodium lead to higher linear power being available and a lower pitch to diameter ratio required [3], [4].

Gr.92 (Ferritic/martensitic steels) is considered as candidates of cladding materials of Sodium-cooled Fast Reactors (SFRs). Its compatibility with sodium is one of issues especially dissolution, chemical reaction, and carbon transfer with impurities, which degraded the mechanical properties. The compatibility of cladding and structural materials with sodium has to be carefully investigated, as sodium could promote corrosion of cladding and structural materials in two ways. One is produced by the dissolution of alloy constituents into the sodium, and the other is produced through a chemical reaction with impurities (especially oxygen and carbon) in the sodium environment [5].

In the Ultra-long Cycle Fast Reactor (UCFR) which is developed in UNIST, cladding is exposed long-term in high temperature liquid sodium environment [6]. So, it is very important to investigate the corrosion-related behavior such as surface corrosion rate, carburization, decarburization and mechanical properties for its operation time.

The decarburization process where dissolved carbon near the specimen surface diffused in to the liquid sodium. This process can originate from the difference between dissolved carbon activity in the material and liquid sodium. A compatibility test the cladding tube revealed that a decrease of the mechanical property instigated by the aging proves governed the whole mechanical property [7].

The materials are exposed to the liquid sodium for long periods, the structural materials experience highly corrosive environments. The increased high temperature of the environment may reduce the margins of safety against failure during normal operation, as well as promoting corrosion [8]–[10].

While nuclear reactor is running, the structure material of a cladding materials will face neutron and multiple types of ion beam irradiations, which will induce the structure damage in the cladding [11]–[13]. Proton irradiation has been used in the past decades to reproduce neutron damage, and protons have a scattering cross-section higher than fast neutrons, and it leading to a displacement rate for nuclear material research [14]–[16]. Besides, The reduction of total elongation is observed to linearly increase by increasing the dose, and significant influence of liquid metal on the tensile properties [17].

In this study, FMS and irradiated FMS were tested as corrosion and dissolution. The combined effect of irradiation and liquid metal corrosion on the FMS will be concluded. Especially, it is aimed to conclude the effect of irradiation conditions on the corrosion rate of the steels in liquid metal environment.

2. Experimental

The composition of the Gr.92 and HT9 used in this experiment is given in table 1. Heat treatment was performed normalizing and tempering. The both specimen was normalized at 1050 °C for 1 hour, followed by air cooling, then tempering at 780 °C for 30 min. The sample was cut into small strips with the size: 10mm×5mm×2mm and further polished successively with 320, 400, 600, and 800 grit polishing paper and diamond polishing until 1 μm. It was cleaned in an ultrasonic cleanser with ethanol, acetone, and distilled water in sequence.

FIG. 1. Chemical composition of the test material (wt.%)

	C	Si	Mn	Cr	Ni	Mo	W	V
Gr.92	0.087	0.21	0.41	8.69	0.13	0.38	1.62	0.18
HT9	0.19	0.14	0.49	12.05	0.48	1.00	0.49	0.30

The proton irradiation experiments were carried out in TR23 (20 MeV) accelerator in KOMAC (Korea Multi-purpose Accelerator Complex), gyeong-ju, Korea. The beam dump of KOMAC is located the photon production downstream are for a continuous absorption of the generated beam energy [18].

In the case of irradiation with 3 MeV protons, the proton fluences were 5×1015#/cm2 and 1016#/cm2, respectively. Those fluences were condition for maximum terms for highest displacement per atom at KOMAC. The stability of the current was within ±5%. The largest average current is 0.6mA, pulse width is 0.05 ms. The total damage and depth of stopping range in the sample, calculated through the Stopping and Range of Ions in Matter (SRIM) code.

The immersion experiment was performed in the glove box in order to examine the effectiveness of irradiation and chrome concentration in specimen as a function of the exposure time. The experimental setup, shown in Fig. 1, had the capability for safety sodium immersion experiment under high temperature and long exposure time. Dissolved oxygen is also saturated in the liquid sodium. Each specimen is taken out 100h, 200h and 300h, respectively.

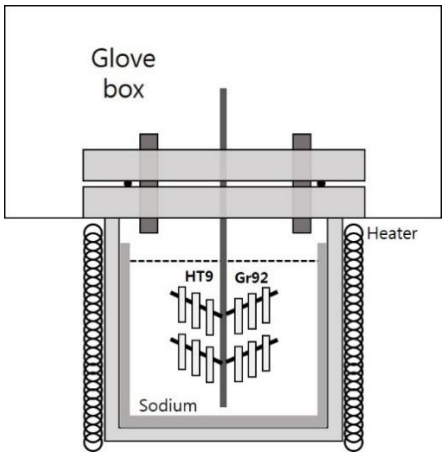

Fig. 1. Schematic of liquid sodium experimental facility,

3. Results and Discussion

The proton irradiation experiment and immersion experiments were conducted for th is study at 2 types of dose rate conditions and various exposure time.

3.1 Irradiation result

Irradiations were conducted using 3 MeV protons, which have a penetration distanc e of 40 μm in stainless steel, to ensure that there was no implantation within the 30 μm sample. An example of the hydrogen profile and dpa profile calculated by the S RIM code is shown in below graph. The damage profile of SRIM simulation is illust rated in Fig.2. The damage profile was fairly flat at an average of 3×10-5 displaceme nts/angstrom-ion. From the SRIM result, it can be verified that the irradiated specime n can be used to immersion test.

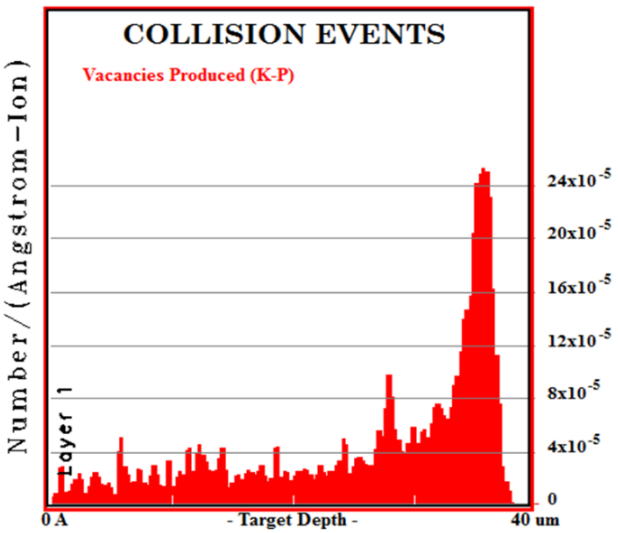

Fig. 2. SRIM result of 3MeV proton beam incident on Gr.92 target. Damage peak occurs a round 38 μm into the sample. Nominal sample thickness of 30 μm was used to avoid the damage peak and any proton implantation,

3.2 Immersion test

Oxygen dissolves in sodium as the monoxide Na2O. Assuming compound formation, we may commence by considering the reaction (Equation (1)). In the liquid sodium environment, NaCrO2 is more stable compound than Na_2O [10]. Na2O encounter electrons, then it forms the NaO_2^{3-} and Na (Equation (2)). And chrome atom emits the electron which is cation (Equation (3)).

And chromium is a strong oxide former, and sodium chromite, NaCrO2, forms readily according to the reaction (Equation (4)). The reaction has been written for Na2O in solution in sodium.

$$2\mathrm{Na(l)} + \frac{1}{2}O_2 \rightarrow Na_2O(s) \quad (1)$$

$$2Na_2O(s) + 3e \rightarrow NaO_2^{3-} + 3Na(l) \quad (2)$$

$$Cr(s) \rightarrow Cr^{3+} + 3e \quad (3)$$

$$2\mathrm{Na}_2O(soln) + Cr(s) \rightarrow NaCrO_2 + 3Na(l) \quad (4)$$

The immersion tests at higher temperature with as-received and irradiated HT9 and Gr.92 specimens are under process and also as-received specimens were exposed to oxygen saturated sodium environment for NaCrO2 formation on the surface

To explain the existence of NaCrO2, EDS analysis is performed with X-ray mappin g analysis and point analysis. In order to confirm the existence of NaCrO2, X-ray ph otoelectron spectroscopy (XPS) analysis was also performed with same specimens. Res ult shows the XPS spectra of specimen after 300 h of exposure time to 650 oC oxyg en-saturated sodium including survey, C1s, O1s, Na1s, and Cr2p spectra, and the resul t confirms the existence of NaCrO2 compound in the surface of specimen.

Figure 4 shows the FIB images of the as-received, 0.006 dpa, and 0.012 dpa speci mens. Dark regions indicate chromium-rich zones, which are ~9.98 μm, ~11.64 μm, a nd 12.32 μm thick in the as-received, 0.006 dpa, and 0.012 dpa specimens, respective ly. The thicknesses of the chromium-rich zones on the as-received specimens are less than that of the irradiated specimen. The chromium-rich zone on the as-received speci men is the thinnest because the specimen damage is relatively small.

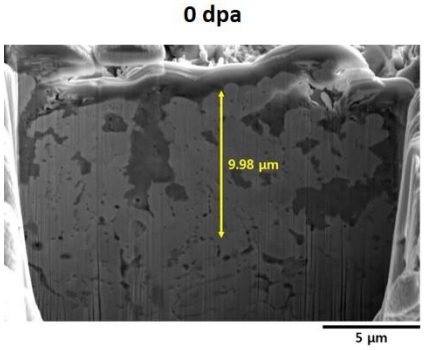

(a)

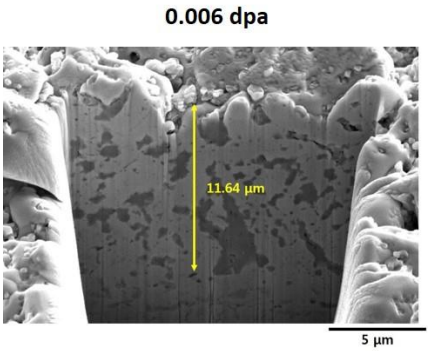

(b)

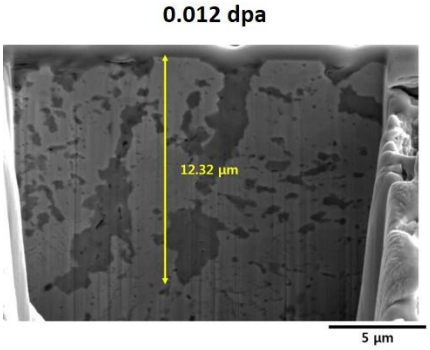

(c)

Fig. 4. FIB-SEM images of (a) as-received, (b) 0.006 dpa damaged specimen, and (c) 0.012 dpa damaged specimen after 300 h exposure in 650 oC oxygen-saturated sodium. The vertical arrow bars indicate the depth of chromium rich zone from the surface of the metal.

3.3 Factor of corrosion acceleration

Figure 5 shows the atomic forced microscopy (AFM) photographs of surface morph ology of specimen before and after H+ ion irradiation. It could be observed from the figure that, after irradiation, both the surface projections and the rms roughness of s pecimen increased. The evolution of ion beam irradiated solid surface was the result of a competition between the roughening process caused by ion bombardment and the smoothing process caused by material transport. It was clear that the roughening pro cess caused by ion bombardment played a dominant role [19]. These results indicate t hat the grain matrices were also heavily attacked by the sodium, and hence that proto n ion irradiation significantly increases intergranular corrosion in the irradiated and cor roded sample. Moreover, a large number of small cavities and NaCrO2 were observed on the surface.

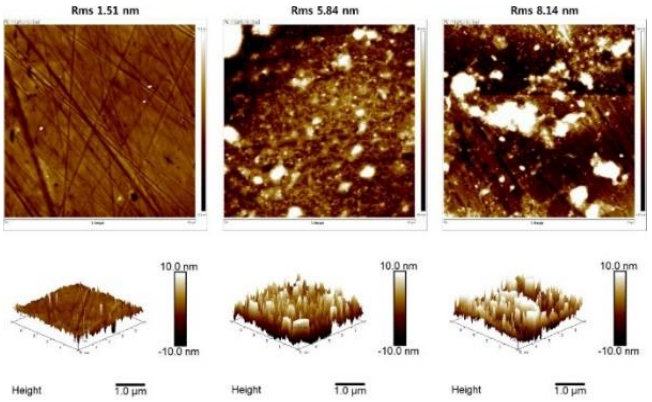

Fig. 5. AFM micrographs showing the change in surface morphology for specimen irradiated by protons with various fluences.

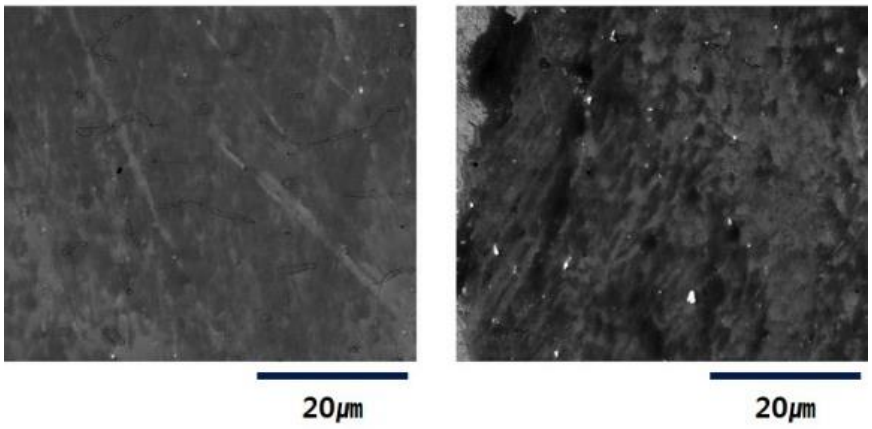

Fig. 6. SEM observation of the Cr-rich phase in the specimen irradiated

Enrichment or depletion of solute in sink, such as grain boundary, by irradiation can lead directly to precipitate formation if the local solute concentration exceeds the solubility limit. Therefore, the precipitation of the materials under irradiation can be an example of radiation-induced precipitation in an undersaturated solid solution. Depending on the amount of proton irradiation, radiation induced precipitation can be increased in the irradiated materials. It can be shown is Fig. 6.

4. Conclusion

In this study, as-received Gr.92 and irradiated Gr.92 specimen in the oxygen-saturated liquid sodium were examined at high temperature for 300h. The microstructure results reveal the information for the effect of irradiation and effect of the chrome concentration in specimen.

i. From the SRIM result, penetration distance of 40 μm in stainless steel and nominal sample thickness of 30 μm was used to avoid the damage peak and any proton implantation

ii. From the microstructural evaluation, chromium-rich zones existed under the surface of the both of non-irradiated and irradiated materials. The irradiated materials showed chromium-rich zones with bigger depths than the non-irradiated specimens.

iii. Also, through the weight loss measurement, it was observed that materials, which has the reduced chromium content by proton irradiation, shows the relatively much weight loss.

iv. Corrosion resistance was degraded with (a) the increased of surface roughness, (b) chromium depletion by radiation induced precipitation, and (c) potential path for corrosion by radiation defect, which are caused by irradiation.

ACKNOWLEDGEMENTS

This work was financially supported by the International Collaborative Energy Technology R&D Program (No. 20168540000030) of the Korea Institute of Energy Technology Evaluation and Planning (KETEP) which is funded by the Ministry of Trade Industry and Energy.

REFERENCES

[1] S. H. Shin, S. H. Kim, and J. H. Kim, “Model of liquid gallium corrosion with austenitic stainless steel at a high temperature,” *J. Nucl. Mater.*, vol. 450, no. 1–3, pp. 314–321, 2014.

[2] P. Problem, L. Coolant, and N. Reactors, “Investigation on the Polonium Problem in Lead-Bismuth Coolant for Nuclear Reactors Sung Il Kim , Kun Jai Lee Korea Advanced Institute of Science and Technology 305 Korea.”

[3] J. Carlsson and H. Wider, “Comparison of sodium and lead-cooled fast reactors regarding reactor physics aspects , severe safety and economical issues,” vol. 236, pp. 1589–1598, 2006.

[4] P. Mazgaj, P. Darnowski, S. Gurgacz, M. Lipka, and K. Dziubanii, “Comparison of Simple Design of Sodium and Lead Cooled Fast Reactor Cores,” vol. 94, pp. 16–26, 2014.

[5] T. Furukawa, S. Kato, and E. Yoshida, “Compatibility of FBR materials with sodium,” *J. Nucl. Mater.*, vol. 392, no. 2, pp. 249–254, 2009.

[6] J. A. Jung, S. H. Kim, S. H. Shin, I. C. Bang, and J. H. Kim, “Feasibility study of fuel cladding performance for application in ultra-long cycle fast reactor,” *J. Nucl. Mater.*, vol. 440, no. 1–3, pp. 596–605, 2013.

[7] J. H. Kim and S. H. Kim, “Microstructure and mechanical property of ferritic-martensitic steel cladding under a 650 C liquid sodium environment,” *J. Nucl. Mater.*, vol. 443, no. 1–3, pp. 112–119, 2013.

[8] M. C. Billone, T. a. Burtseva, and R. E. Einziger, “Ductile-to-brittle transition temperature for high-burnup cladding alloys exposed to simulated drying-storage conditions,” *J. Nucl. Mater.*, vol. 433, no. 1–3, pp. 431–448, 2013.

[9] S. H. Shin *et al.*, “Measurement of Emf in Liquid Sodium Using a Gadolinia-Doped Ceria Solid Electrolyte,” *J. Electrochem. Soc.*, vol. 162, no. 7, pp. B152–B158, 2015.

[10] J. Lee, S. H. Shin, J. K. Lee, S. Choi, and J. H. Kim, “Corrosion behavior of surface treated steel in liquid sodium negative electrode of liquid metal battery,” *J. Power Sources*, vol. 307, pp. 526–537, 2016.

[11] W. J. S. Yang, “PRECIPITATE STABILITY IN NEUTRON-IRRADIATED 0022-3115 / 88 / $ 03 . 50 0 Elsevier Science Publishers B . V . (North-Holland Physics Publishing Division),” *J. Nucl. Mater.*, vol. 158, pp. 71–80, 1988.

[12] G. E. Lucas, M. Surprenant, J. Dimarzo, and G. J. Brown, “Proton irradiation creep of Zircaloy-2,” *J.*

Nucl. Mater., vol. 101, pp. 78–91, 1981.
[13] J. J. Kai, W. I. Huang, and H. Y. Chou, "The microstructural evolution of zircaloy-4 subjected to proton irradiation," *J. Nucl. Mater.*, vol. 170, no. 2, pp. 193–209, 1990.
[14] H. H. Shen, S. M. Peng, X. Xiang, F. N. Naab, K. Sun, and X. T. Zu, "Proton irradiation effects on the precipitate in a Zr–1.6Sn–0.6Nb–0.2Fe–0.1Cr alloy," *J. Nucl. Mater.*, vol. 452, no. 1–3, pp. 335–342, 2014.
[15] L. Tournadre *et al.*, "Experimental study of the nucleation and growth of c-component loops under charged particle irradiations of recrystallized Zircaloy-4," *J. Nucl. Mater.*, vol. 425, no. 1–3, pp. 76–82, 2012.
[16] L. Tournadre *et al.*, "Toward a better understanding of the hydrogen impact on the radiation induced growth of zirconium alloys," *J. Nucl. Mater.*, vol. 441, no. 1–3, pp. 222–231, 2013.
[17] E. Stergar, M. Lambrecht, and S. Gavrilov, "Comparison of the mechanical properties of T91 steel from the MEGAPIE , and TWIN-ASTIR irradiation programs," vol. 468, pp. 228–231, 2016.
[18] J. Kim, C. S. Gil, W. Maeng, and D. Kim, "Design of a high energy proton beam dump for KOMAC," *Nucl. Instruments Methods Phys. Res. Sect. A Accel. Spectrometers, Detect. Assoc. Equip.*, vol. 562, no. 2, pp. 997–1000, 2006.
[19] H. Zhang, X. Mei, Y. Wang, Z. Wang, and Y. Wang, "Resistance to H + induced irradiation damage in metallic glass," *J. Nucl. Mater.*, vol. 456, no. August 2014, pp. 344–350, 2015.